SSRG International Journal of Mechanical Engineering
ISSN: 2348-8360/ https://doi.org/10.14445/23488360/IJME-V12I11P102

Volume 12 Issue 11, 14-22, November 2025

Original Article

Numerical Investigation of Wet Steam Condensation in Low-Pressure Turbine Blades

Eder Martínez-Sandoval[1], Laura Castro[1], Juan Carlos García[1*], Rogelio Martinez-Oropeza[1], José Cubos-Ramirez[1], Dulce. Graciano[1], José. Dávalos[2]

[1] *Centro de Investigación en Ingeniería y Ciencias Aplicadas (CIICAp), Universidad Autónoma del Estado de Morelos (UAEM), Morelos, México.*
[2]*Departamento de ingeniería Industrial y Manufactura, Universidad Autónoma de Ciudad Juárez, Chihuahua, México.*

[*]*Corresponding Author : jcgarcia@uaem.mx*

Received: 03 September 2025 Revised: 04 October 2025 Accepted: 05 November 2025 Published: 28 November 2025

Abstract *- In this work, the phase change of steam in the last stage of a turbine was investigated, since the formation of water droplets causes structural damage to the blades, affecting power output and efficiency, as well as increasing operation and maintenance costs. Therefore, this work uses Computational Fluid Dynamics (CFD) to study the low-pressure stage where the condensation phenomena occurred, and the phase change is analyzed by varying the vacuum pressure in the discharge of the turbine. The case study corresponds to the low-pressure stage of a 110 MW steam turbine with 0.8 m blades, which operates under vacuum pressures and low temperatures. The CFD computations are carried out in a 2D and 3D geometric model of the last stage of the steam turbine, using the Spalart-Allmaras turbulence model, the wet steam model (to solve the phase change), and the simple reference frame technique (to simulate blade movement). The results enabled the determination of the spatial distribution of the phase change along the section of the last stage of the turbine. They were validated against data available in the literature. The magnitude of the phase change was evaluated as a function of the steam outlet pressure for all evaluated conditions. Showing that the phase change occurs from the center toward the outlet of the blades of the last stage.*

Keywords *- CFD, Change Phase, Nozzle, Steam Turbine, Wet Steam.*

1. Introduction

Steam turbines are essential components in power plants, as they convert the thermal energy of steam into mechanical energy to drive electric generators. During this process, high-pressure, high-temperature steam passes through the different stages of the turbine, transferring kinetic energy to the blades attached to the rotor. Within these stages, the last stage (low-pressure stage) plays a crucial role in the overall performance of the turbine. Due to its operating conditions, this stage is highly susceptible to phase change, causing the steam to condense into liquid droplets as the pressure and temperature decrease during expansion. These droplets are carried by steam at high speeds and strike the blades, causing significant thermodynamic losses [1], reduced efficiency and power output [2], and severe blade erosion [3-7], all of which increase operating and maintenance costs.

The flow field in the last stage of a steam turbine is highly complex due to the large size of the blades and the high speeds reached near the tips, favouring the development of non-stationary three-dimensional structures that directly influence the occurrence of condensation phenomena. Therefore, it is vitally important to understand the magnitude of the phase change in the low-pressure stage as a function of the steam outlet pressure to minimize the damage associated with this phenomenon. One of the first studies on steam condensation was based on the theory of homogeneous nucleation, initially proposed by V. K. Oswatitsch [8] and later developed by J. Frenkel [9], W. J. Dunning [10], and J. E. McDonald [11] as the theory of critical droplet formation in pure steam. With the same objective, experimental research has been reported on the phenomenon of wet steam flow nucleation, mainly in nozzles and low-pressure steam turbine covers [12, 13]. Noteworthy is the work carried out by F. Bakhtar et al. [14, 16], in which they measured the pressure distribution, the onset of nucleation, and the growth of droplets in wet steam flows. Other studies, such as those by G. Zhang et al. [17-20], focused on optimizing blade design to reduce condensation regions by inserting a flow channel into the steam turbine blade, while L. Cao et al. [21] applied models of two-phase flow, homogeneous nucleation, and droplet growth, demonstrating that vortex formation and flow field parameters influence the location of condensation, as well as the number and size of droplets. Although these studies have contributed to the understanding of the phenomenon, numerical studies make assumptions that do

not consider the three-dimensional and unsteady behaviour of the last stage.

Similarly, C. Wen et al. [22] developed a numerical study to understand steam condensation on turbine blades, comparing their results with experimental data reported in the literature. The results showed that steam subcooling can reach up to 50 K and that liquid humidity can reach 5%.

The use of Computational Fluid Dynamics (CFD) has enabled a more detailed analysis of the multiphase phenomena that occur in steam turbines. Several CFD-based studies [23, 24] have addressed the prediction of condensation initiation and droplet growth. However, few have focused on three-dimensional analyses of the last stage of the turbine under varying vacuum conditions at the outlet.

This article presents a numerical study of the low-pressure stage of a 110 MW steam turbine to identify the regions where droplet formation begins and evaluate the impact of outlet vacuum pressure on flow behavior, efficiency, and power generation. It should be noted that the 110 MW turbine was previously analyzed by JC García et al. using 2D CFD simulations to determine the pressure fields on the blades and to determine the forces on the blades resulting from flow variations in the rotor-stator assembly with axial clearance.

2. Governing Equations and Mathematical Model

The numerical simulation of phase change was performed using 2D and 3D geometric models of the last stage of a steam turbine. Two case studies were considered: the first in a cross-section at an average height of the nozzle and blades, and the second across the entire 3D surface of the nozzle and blades. The computational domain was divided into two regions: the stationary nozzle section and a rotating blade section operating at a known angular velocity.

To solve turbulence in the flow domain, Reynolds Averaged Navier-Stokes (RANS) equations were used, solved using the Spalart-Allmaras (S-A) turbulence model. In addition, a wet steam model was employed to analyze the phase change, while the simple reference frame technique was used to simulate the blade movement. The Navier-Stokes equations and the continuity equation describe the dynamics of continuous fluids, Equation (1) [25, 26].

$$\frac{\partial}{\partial t}(\rho u_i) - \frac{\partial}{\partial x_j}(\rho u_i u_j) = -\frac{\partial p}{\partial x_i} + \frac{\partial}{\partial x_j}\left(\mu \frac{\partial u_i}{\partial x_j}\right) + \frac{1}{3}\frac{\partial}{\partial x_i}\left(\mu \frac{\partial u_j}{\partial x_j}\right) \quad (1)$$

Where μ is the viscosity, ρ the density, ui the velocity in direction i, and P the pressure.

To solve the Navier-Stokes equations in regions with rotation, it is necessary to include an additional term to consider the acceleration of the fluid in the rotating zones. In a rotating region, the absolute velocity (u) and relative velocity (ur) of the fluid are given by Equation (2).

$$u_r = u - (\Omega \times r) \quad (2)$$

Where r is the position vector of the rotating domain and Ω is the angular velocity vector.

The continuity equation can be solved in terms of absolute velocity or relative velocity. However, the momentum equation must include the relative velocity, angular velocity, and the effect of Coriolis forces- Equation (3).

$$\frac{\partial}{\partial t}(\rho u_i) + \frac{\partial}{\partial x_j}(\rho u_{ri} u_j) + \rho(\Omega \times u_i) = -\frac{\partial p}{\partial x_i} + \frac{\partial}{\partial x_j}\left(\mu \frac{\partial u_i}{\partial x_j}\right) + \frac{1}{3}\frac{\partial}{\partial x_i}\left(\mu \frac{\partial u_j}{\partial x_j}\right) \quad (3)$$

2.1. Turbulence Modelling

The Spalart-Allmaras turbulence model is a one-equation model. This model solves a single scalar transport equation for kinematic viscosity (eddy viscosity) and employs several parameters and coefficients. This model was designed for aerodynamic applications. However, it has demonstrated satisfactory results in engineering flows, particularly turbomachinery. The scalar transport equation used is defined by Equation (4).

$$\frac{\partial}{\partial t}(\rho \tilde{v}) + \frac{\partial}{\partial x_i}(\rho \tilde{v} u_i) = G_v + \frac{1}{\sigma_{\tilde{v}}}\left[\frac{\partial}{\partial x_j}\left\{(\mu + \rho \tilde{v})\frac{\partial \tilde{v}}{\partial x_j}\right\} + C_{b2}\rho\left(\frac{\partial \tilde{v}}{\partial x_j}\right)^2\right] - Y_v + S_{\tilde{v}} \quad (4)$$

Where G_v Is the production of turbulent viscosity, and Y_v This is the turbulent viscosity destruction that occurs in the near-wall region. $\sigma_{\tilde{v}}$ and C_{b2} are the constants, and v is the molecular kinematic viscosity. $S_{\tilde{v}}$ It is a user-defined source term.

The turbulent viscosity μ_t is defined by Equation (5).

$$\mu_t = \rho \tilde{v} f_{v1} \quad (5)$$

Where the damping function, f_{v1} is defined by Equation (6).

$$f_{v1} = \frac{X^3}{X^3 + C_{v1}^3} \quad (6)$$

$$X \equiv \frac{\tilde{v}}{v}$$

The production term, G_v It is modeled by Equation (7).

$$G_v = C_{b1}\rho\tilde{S}\tilde{v} \quad (7)$$

$$\tilde{S} \equiv S + \frac{\tilde{v}}{k^2 d^2} f_{v2} \quad (8)$$

$$f_{v2} = 1 - \frac{X}{1+Xf_{v1}} \quad (9)$$

C_{b1} and k are empirical constants, d is defined as the n ormal distance from the wall, and S represents a scalar meas ure of the deformation tensor. It is based on the magnitude o f the vorticity expressed by Equation (10).

$$S \equiv \sqrt{2\Omega_{ij}\Omega_{ij}} \quad (10)$$

Where, Ω_{ij} It is defined as the mean rate-of-rotation ten sor. Expressed by Equation (11).

$$\Omega_{ij} = \frac{1}{2}\left(\frac{\partial u_i}{\partial x_j} - \frac{\partial u_j}{\partial x_i}\right) \quad (11)$$

2.2. Multiphase Flow Model

Wet steam is a mixture of two phases. The gaseous phase consists of water vapor, and the liquid phase consists of condensed water droplets. The following assumptions are made for the model solution:

- The velocity slip between the droplets and the gaseous p hase is negligible.
- Droplet–droplet interactions are neglected.
- The mass fraction of the liquid phase (y_l) is small (<1%)
- The droplet volume is negligible due to their small size (0.1–100 µm).

From the preceding assumptions, it follows that the mixture density (ρ_m) can be related to the vapor density (ρ_v) by Equation (12).

$$\rho_m = \rho_v + y_l(\rho l - \rho_v), \quad (12)$$

Where the liquid density is ρl, the pressure and temperature of the mixture are taken as equal to those of the vapor phase. The equations governing the flow of a compressible mixture are the Navier-Stokes equations in conservative form, expressed in Equation (13).

$$\frac{\partial Q}{\partial t} + \nabla \cdot FQ = S(Q) \quad (13)$$

Where Q represents mixture variables.

To model wet steam, two additional transport equations were used. The first transport equation governs the mass fraction of the condensed liquid phase by Equation (14), and the second governs the number density of droplets per unit volume, Equation (15).

$$\frac{\partial y_l}{\partial t} + u_j \frac{\partial y_l}{\partial x_j} = \dot{m} \quad (14)$$

$$\frac{\partial n}{\partial t} + u_j \frac{\partial n}{\partial x_j} = J \quad (15)$$

Where $\dot{m}$ Is the condensation/evaporation mass generation rate (kg per unit volume per second), and J is the nucleation rate (number of new droplets per unit volume per second). The number of droplets per unit volume N is given by Equation (16), being r_d The average radius of the drops.

$$N = \frac{3y_l}{4\pi r_d^3} \quad (16)$$

3. Geometry and Boundary Conditions

3.1. Geometry

The last stage of a 110 MW steam turbine was considered for the present study. This stage has a mean radius of 1.12 m with a stator composed of 55 nozzles and a rotor with 110 blades. The CFD simulations consider only a representative section of the stage consisting of a nozzle and two blades, both with the same circumference. It is necessary to mention that the periodic boundary conditions were used on every side of the stage segment. The 2D simulations were carried out in the middle plane, corresponding to 0.6m from the hub, as shown in Figure 1.

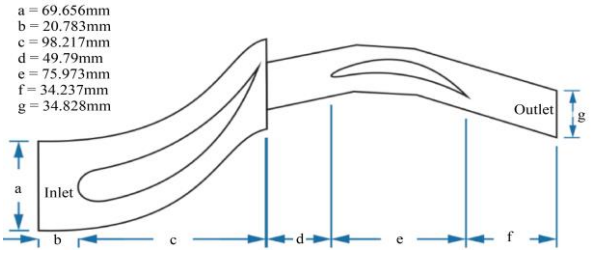

Fig. 1 Geometric aspects of the 2D stage turbine [4].

The mesh for 3D simulations was constructed with 324,555 quadrilateral-type cells, with a minimum size of 3.62x10 $^{-4}$ m² and a maximum of 4.82x10 $^{-4}$ m². The mesh specifications for the 2D study were the same. Figure 2 shows the meshes used for this study.

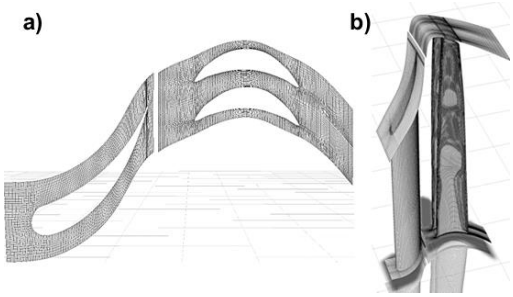

Fig. 2 Mesh for simulation (a) 2D model, and (b) 3D model.

3.2. Boundary Conditions

The phase change in the last stage was calculated using the wet steam approach, considering normal operating conditions and off-design operating conditions, with discharge pressures ranging from 85% to 115% of the normal condition. Table 1 summarizes the inlet and outlet conditions for the different discharge pressures.

Table 1. Boundary conditions of the low-pressure stage for different discharge pressures

Vacuum pressure (%)	Inlet pressure (KPa)	Inlet temperature (K)	Outlet pressure (KPa)
85	28.61	341	9.54
90	28.61	341	10.10
95	28.61	341	10.66
100**	28.61	341	11.23
105	28.61	341	11.79
110	28.61	341	12.35
115	28.61	341	12.91

***Design Conditions*

4. Validation of the Numerical Method

The validation of the numerical method was based on a study presented by C. A. Moses and G. D. Stein in 1978, in which experimental data on the phase change of steam that passes through a nozzle were obtained. The numerical results obtained from the methodology validation are analyzed through contours and profiles of velocity, pressure, and droplets per unit volume.

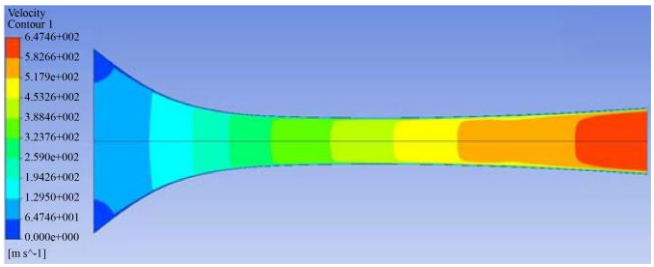

Fig. 3 Contours of velocity calculated on the nozzle studied by C. A. Moses and G. D. Stein

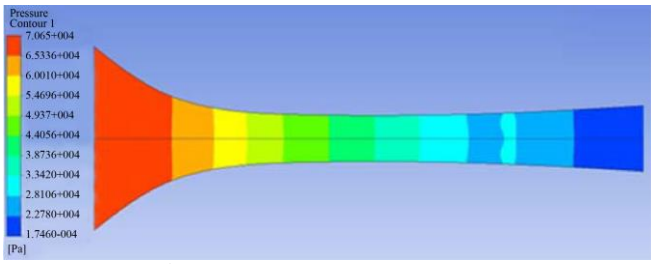

Fig. 4 Contours of static pressure on the nozzle studied by C. A. Moses and G. D. Stein

In Figure 3, the behaviour of the absolute velocity inside the nozzle is studied by C. A. Moses and G. D. Stein. It can be seen that the velocity increases as the steam flow passes through the nozzle, reaching a greater magnitude at the outlet. The corresponding pressure profile (Figure 4) shows the pressure drop along the nozzle, consistent with the steam expansion process.

Figure 5 compares the steam expansion calculated by the wet steam model, without the wet steam model, and the experimental measurements. The results obtained with the wet steam model show excellent agreement with the experimental data reported by C. A. Moses and G. D. Stein, achieving a relative error of 2.88% and accurately capturing both the trend and the magnitude of the expansion process. In this figure, the values of the static pressure shown are dimensionless with respect to the stagnation pressure (P/Po) [27, 28]. Given the strong agreement between the numerical and experimental results, the proposed mesh is considered adequate to represent the flow behavior and expansion process in the nozzle.

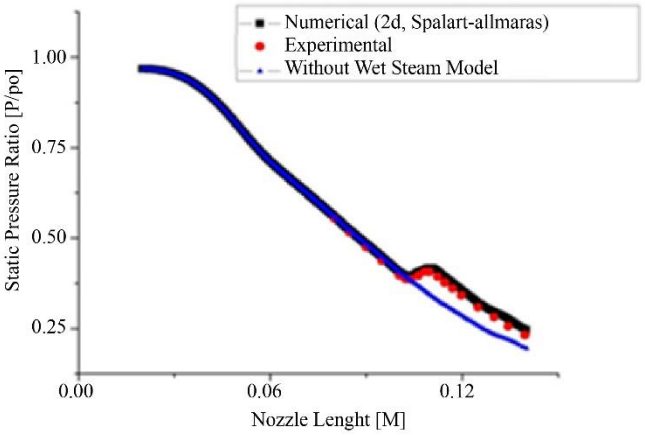

Fig. 5 Comparison of pressure profiles with and without the wet steam model and experimental measurements reported by C. A. Moses and G. D. Stein

Figure 6 shows the contours of the number of drops per unit volume. It can be observed that the quantity of drops is presented after the minimum throat and up to the outlet of the nozzle. After the minimum throat occurs, the expansion contributes to the cooling of the steam and the phase change [5, 29].

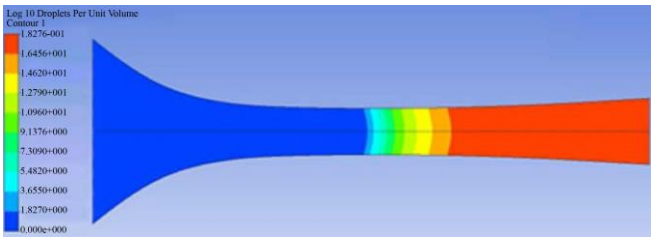

Fig. 6 Contours of droplets per unit volume on the nozzle

5. Results and Discussion

Having validated the CFD model against the experimental data, the wet steam model was applied to the

last stage of a 110 MW steam turbine under normal operating conditions and for different vacuum conditions at the output. For all simulations, the Spalart-Allmaras turbulence model and steam phase change model were used.

5.1. Results for Normal Operating Conditions

Figure 7 shows that the static pressure obtained in the 2D study reaches its maximum value at the inlet, mainly at the leading edge of the blade, registering 29,463.81 Pa. Subsequently, it decreases along the axial direction until reaching a lower value in the minimum throat section of the blades, with 10,324.10 Pa.

Fig. 7 Contours of static pressure at the last stage of the steam turbine in a 2D study

Figure 8 shows the pressure contours of the last stage of the turbine in 3D. Here, it is observed that pressure along the entire surface is not uniform, which is attributed to the geom etric design of the nozzle and blades. However, the pressure distribution behaves similarly in the two-dimensional simula tion, with the highest value recorded at the leading edge of t he blade at the inlet.

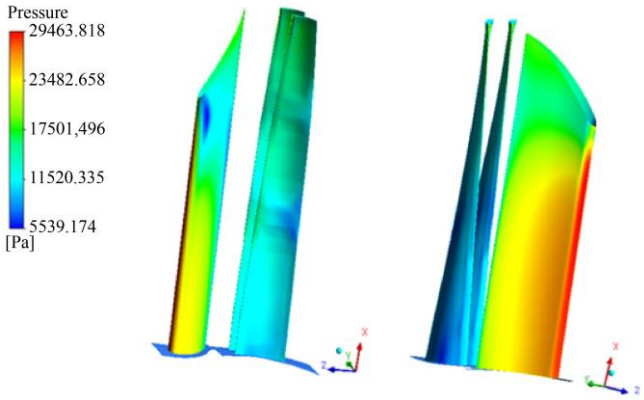

Fig. 8 Contours of static pressure at the last stage of the steam turbine in a 3D study

With respect to the temperature behaviour in the last stage of the steam turbine, the temperature contours obtained in the 2D study (Figure 9) show higher values at the inlet, which decrease along the axial direction until reaching a minimum in the middle zone of the outlet blades. Once the flow passes through the blades, the temperature increases again due to the release of latent heat associated with the phase change of the flow.

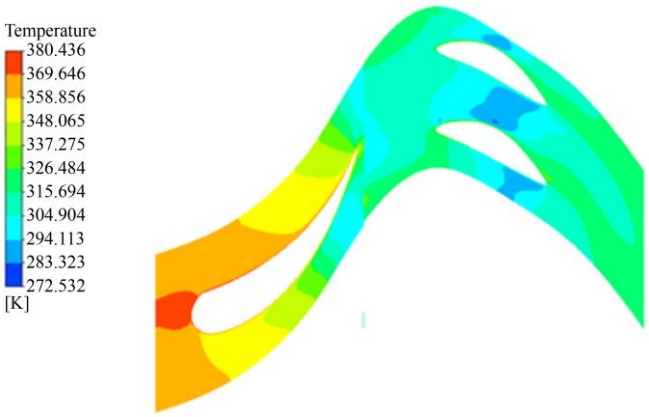

Fig. 9 Contours of temperature at the last stage of the steam turbine in a 2D study

Figure 10 shows the 3D temperature contours with the two different positions of the nozzle and vanes (a), as well as the plane located downstream of the outlet edge (b). The latter illustrates the temperature distribution in the wake of the flow resulting from the phase change.

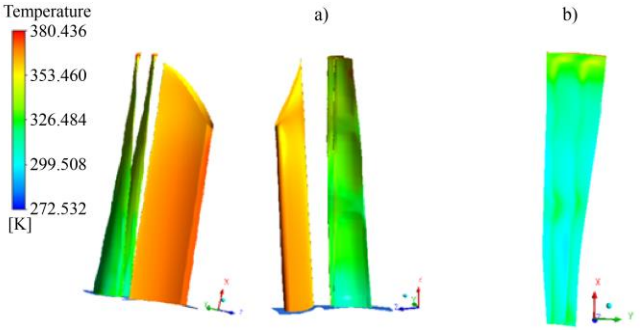

Fig. 10 Contours of temperature at the last stage of the steam turbine in a 3D study, (a) with different positions between nozzle and vanes, and (b) plane located after the exit edges of the vanes.

To understand the flow velocity behaviour in the last stage of the steam turbine, 2D and 3D velocity contours and vectors were used.

Figure 11 shows the 2D velocity contours. In terms of the absolute fluid velocity for the nozzle area, and in terms of the relative velocity of the rotor with respect to the fluid for the blade section, this figure shows that, in the nozzle, the fluid velocity increases as it passes through the section, reaching its maximum value at the minimum throat (562.57 m/s). In the rotor section, a small wake forms at the trailing edge of the blades, which is consistent with the expected aerodynamic behavior of the stator-rotor system. The effect

of the wake can be better appreciated by viewing the vertical plane located after the blade exit, shown in Figure 12.

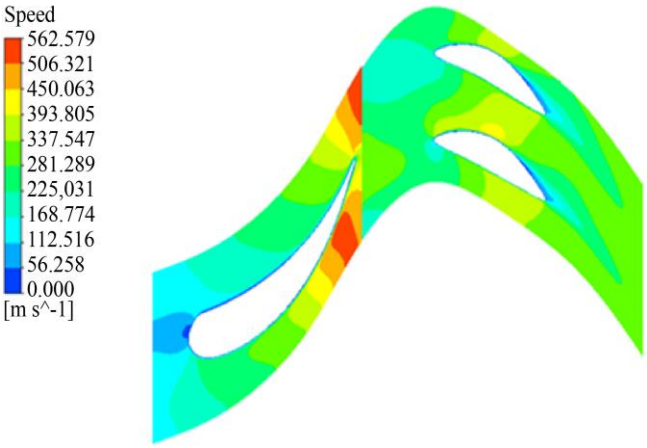

Fig. 11 Velocity contours of the last stage of a steam turbine in a 2D study

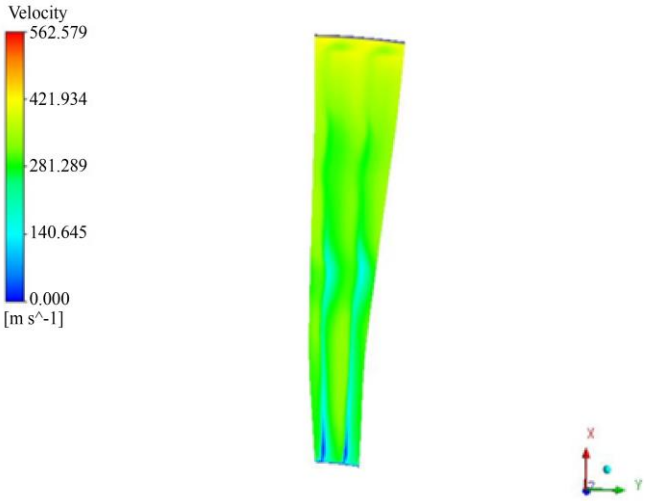

Fig. 12 Velocity contours at a vertical plane after the trailing edges of the blades

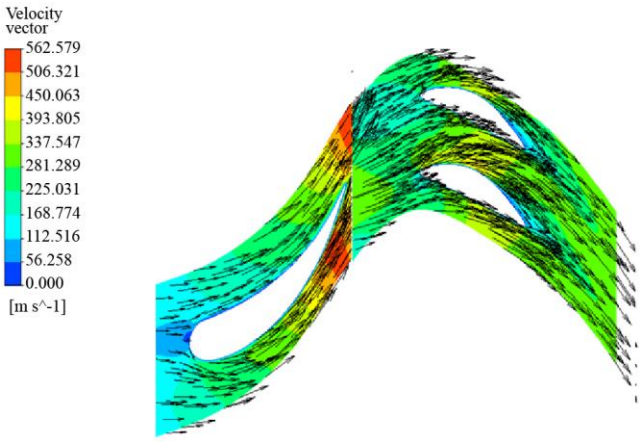

Fig. 13 Vectors of absolute and relative velocity for the last stage of a steam turbine in a 2D study

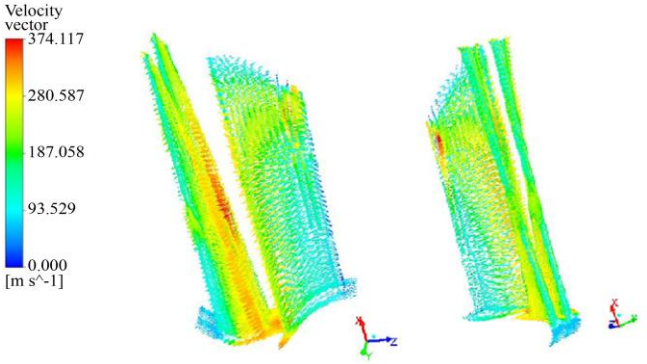

Fig. 14 Vectors of absolute and relative velocity for the last stage of a steam turbine in a 3D study

In the same way that velocity contours are displayed, absolute velocity vectors are used for the nozzle section and relative velocity vectors for the blade section. Figure 13 shows that the absolute velocity vectors are aligned with the shape of the nozzle, which serves to redirect the flow, and the relative velocity vectors are aligned with the shape of the blades. In addition, the fluid velocity increases as it passes through the last stage of the turbine. This behaviour of the vectors at each stage is observed throughout the 3D domain, as shown in Figure 14.

According to the results obtained with the numerical calculation, a phase change of the steam occurs in the last stage of the turbine. To increase understanding of the phenomenon, 2D and 3D contours of the number of droplets per unit volume and the liquid mass fraction are presented.

When analysing Figure 15, it can be seen that the number of droplets per unit volume increase along the nozzle and reach a maximum value just after passing the half of the chord length of the blades, according to the colour map there are up to 1.23 (log10 (17)) drops per cubic meter of the steam flow that runs through the study domain.

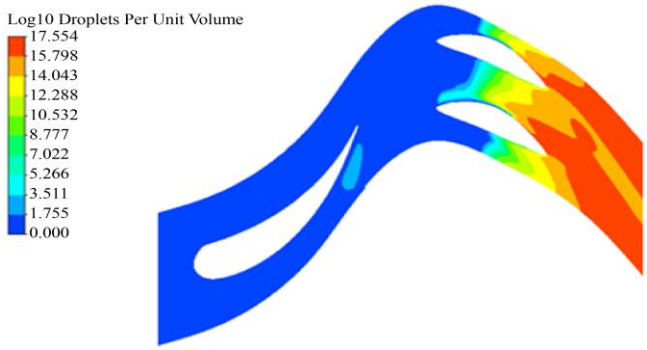

Fig. 15 Contours of droplets per unit volume at the last stage of the steam turbine in a 2D study

Figure 16 shows the contours of the number of drops per unit volume in 3D, in a) the nozzle and vanes are shown in two different positions, while in b) the vertical plane located

after the exit edge of the blades, where you can see that the amount of drops per unit volume is in greater quantity after the trailing edge of the blades.

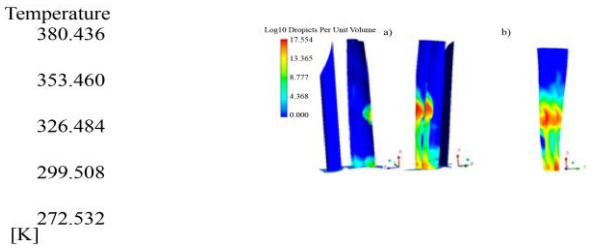

Fig. 16 Contours of droplets per unit volume at the last stage of the steam turbine in a 3D study, (a) with different positions between nozzle and vanes, and (b) plane located after the exit edges of the blades.

The liquid mass fraction increases as it reaches the outlet of the blades, while it is practically zero from the nozzle to the first half of the blade chord, as shown in Figure 17. These results are consistent, since, as the pressure and temperature decrease, the quality of the steam is lower, producing a phase change, but this occurs after the trailing edge of the blades.

Fig. 17 Contours of liquid mass fraction at the last stage of the steam turbine in a 2D study

When viewing the contours of the liquid mass fraction on a vertical plane (Figure 18), located behind the rear edge of the blades, it is confirmed that the volume of liquid will not impact or damage the blades, as the wet vapor occurs after the blade section.

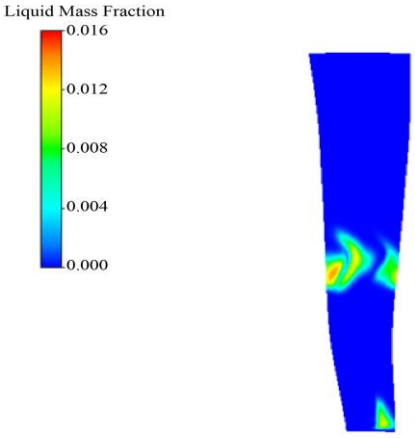

Fig. 18 Contour of the liquid mass fraction, in a vertical plane after the exit edges of the blades in a 3D study

5.2. Results for Different Vacuum Conditions at the Output of the Turbine

Figure 19 shows the static pressure profiles under different vacuum pressure conditions. The results indicate that the static pressure decreases throughout the stage, reaching its minimum at the blade outlet. At this location, a lower vacuum pressure causes an additional reduction in flow pressure. This reduction in static pressure at the outlet increases the fluid velocity. In addition, the behaviour of the liquid mass fraction is closely related to the discharge pressure: as the vacuum pressure decreases, the liquid mass fraction increases (Figure 20).

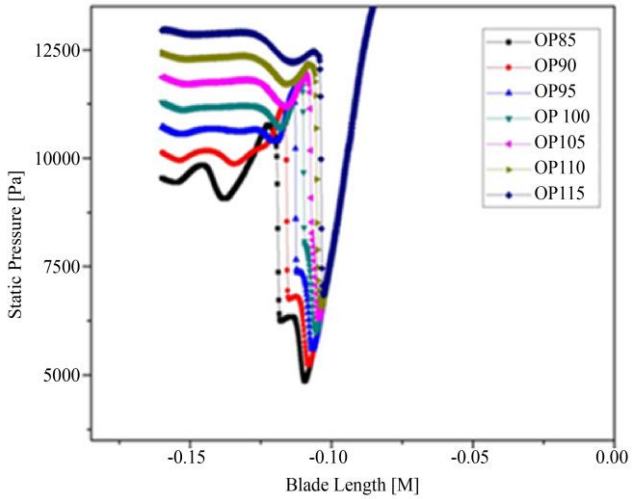

Fig. 19 Static pressure profiles at different vacuum pressures

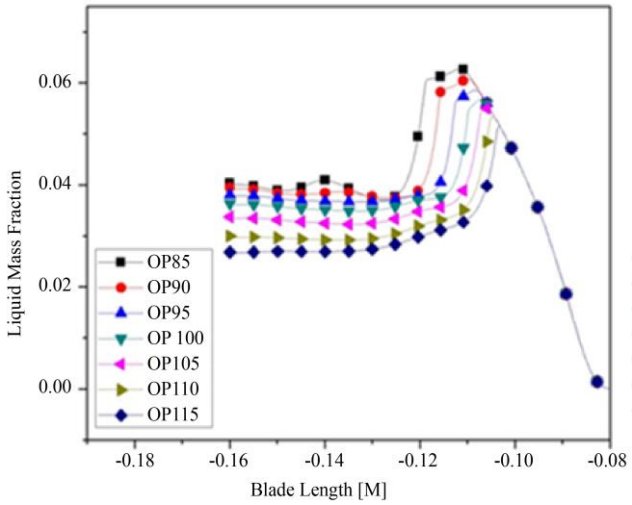

Fig. 20 Liquid mass fraction profiles for different vacuum pressures

6. Conclusion

The phase change in the low-pressure section of a 110 MW steam turbine under different outlet vacuum pressures was investigated using CFD. The simulations enabled the quantification of condensation as a function of outlet pressure

and the identification of regions where droplet formation initiates. The results show that as the outlet pressure decreases, the fluid velocity increases, and condensation is favoured in the last stage. In this sense, pressure and temperature are directly proportional, while velocity is inversely proportional to pressure.

The numerical results confirmed that pressure and temperature exhibit similar trends throughout the stage, with relative deviations of less than 1% from the leading edge of the nozzles to beyond the trailing edge of the blades. No condensation was observed in the nozzles under the studied conditions; nucleation begins downstream of the blade's trailing edge. In this region, the droplet density reached values of up to 1.23 (log10 (17)) droplets/m³ /m³, while the liquid mass fraction reached its maximum at the blade outlet. The results also establish that pressure is inversely proportional to the liquid mass fraction.

Under design operating conditions, no phase change was observed inside the nozzles, ensuring that droplets do not impact directly on the blades, thus preventing erosion and structural damage. Under all operating conditions analyzed, condensation consistently occurred from the middle of the chord to the blade outlet, highlighting the importance of controlling the vacuum pressure at the outlet to mitigate condensation and associated losses.

The results obtained provide a helpful reference framework for optimizing turbine performance under different vacuum pressures and improving maintenance strategies. By identifying the areas where condensation begins and intensifies, solutions can be proposed to prevent blade erosion and associated efficiency losses.

Acknowledgments

All authors contributed equally to the completion of this work.

References

[1] D.E Bohn, N. Sürken, and F. Kreitmeier et al., "Nucleation Phenomena in a Multi-Stage Low Pressure Steam Turbine," *Proceedings of the Institution of Mechanical Engineers, Part A: Journal of Power and Energy*, vol. 217, no. 4, pp. 453-460, 2003. [CrossRef] [Google Scholar] [Publisher Link]

[2] M. Ahmad, M. Schatz, and M.V. Casey, "Experimental Investigation of Droplet Size Influence on Low Pressure Steam Turbine Blade Erosion," *Wear*, vol. 303, no. 1, pp. 83-86, 2013. [CrossRef] [Google Scholar] [Publisher Link]

[3] H. Bagheri Esfe, M.J. Kermani, and M. Saffar Avval, "Effects of Surface Roughness on Deviation Angle and Performance Losses in Wet Steam Turbines," *Applied Thermal Engineering*, vol. 90, pp. 158-173, 2015. [CrossRef] [Google Scholar] [Publisher Link]

[4] S.M.A. Noori Rahim Abadi et al., "CFD-based Shape Optimization of Steam Turbine Blade Cascade in Transonic Two Phase Flows," *Applied Thermal Engineering*, vol. 112, pp. 1575-1589, 2017. [CrossRef] [Google Scholar] [Publisher Link]

[5] Hasril Hasini, Mohd. Zamri Yusoff, and Norhazwani Abd. Malek, *Numerical Modeling of Wet Steam Flow in Steam Turbine Channel*, Mechanical Engineering, pp. 1-22, 2012. [CrossRef] [Google Scholar] [Publisher Link]

[6] Lihua Cao et al., "Numerical Analysis on Spontaneous Condensation Characterization in 3D Twisted Blade Cascade of an Ultra-Supercritical Steam Turbine," *International Communications in Heat and Mass Transfer*, vol. 168, 2025. [CrossRef] [Google Scholar] [Publisher Link]

[7] Nobuyuki Fujisawa, "Review: Fundamentals of Liquid Droplet Impingement and Rain Erosion of Wind Turbine Blade," *Next Energy*, vol. 8, pp. 1-10, 2025. [CrossRef] [Google Scholar] [Publisher Link]

[8] Kl. Oswatitsch, "Condensation Phenomena in Supersonic Nozzles," *ZAMM-Journal of Applied Mathematics and Mechanics*, vol. 22, no. 1, pp. 1-14, 1942. [CrossRef] [Google Scholar] [Publisher Link]

[9] Yakov Il'ich Frenkel, *Kinetic Theory of Liquids*, Oxford University Press, pp. 1-488, 1946. [CrossRef] [Google Scholar] [Publisher Link]

[10] W.J. Dunning, C. Zettlemoyer, and Marcel-Dekker, "General and Theoretical Introduction," *Nucleation*, pp. 1-67, 1969. [Google Scholar]

[11] James E. McDonald, "Homogeneous Nucleation of Vapor Condensation. I. Thermodynamic Aspects," *American Journal of Physics*, vol. 30, no. 12, pp. 870-877, 1962. [CrossRef] [Google Scholar] [Publisher Link]

[12] Dieter E. Bohn, and Husnu Kerpicci, "Nucleation of Droplets and Homogeneous Condensation in an LP-Steam Turbine," *Progress in Computational Fluid Dynamics, an International Journal*, vol. 1, no. 4, pp. 169-177, 2001. [CrossRef] [Google Scholar] [Publisher Link]

[13] J.B. Young, "Two-Dimensional, Nonequilibrium, Wet-Steam Calculations for Nozzles and Turbine Cascades," *Journal of Turbomachinery*, vol. 114, no. 3, pp. 569-579, 1992. [CrossRef] [Google Scholar] [Publisher Link]

[14] F. Bakhtar et al., "On the Performance of a Cascade of Improved Turbine Nozzle Blades in Nucleating Steam. Part 1: Surface Pressure Distributions," *Proceedings of the Institution of Mechanical Engineers, Part C: Journal of Mechanical Engineering Science*, vol. 223, no. 8, pp. 1903-1914, 2009. [CrossRef] [Google Scholar] [Publisher Link]

[15] F. Bakhtar, Z.A. Mamat, and O.C. Jadayel, "On the Performance of a Cascade of Improved Turbine Nozzle Blades in Nucleating Steam. Part 2: Wake Traverses," *Proceedings of the Institution of Mechanical Engineers, Part C: Journal of Mechanical Engineering Science*, vol. 223, no. 8, pp. 1915-1929, 2009. [CrossRef] [Google Scholar] [Publisher Link]

[16] F. Bakhtar, S.Y. Rassam, and G. Zhang, "On the Performance of a Cascade of Turbin Rotor Tip Section Blading in Wet Steam Part 4: Droplet Measurements," *Proceedings of the Institution of Mechanical Engineers, Part C: Journal of Mechanical Engineering Science*, vol. 213, no. 4, pp. 343-353, 1999. [CrossRef] [Google Scholar] [Publisher Link]

[17] Guojie Zhang et al., "Effect Evaluation of a Novel Dehumidification Structure based on the Modified Model," *Energy Conversion and Management*, vol. 159, pp. 65-75, 2018. [CrossRef] [Google Scholar] [Publisher Link]

[18] Guojie Zhang et al., "Numerical Study of the Dehumidification Structure Optimization based on the Modified Model," *Energy Conversion and Management*, vol. 181, pp. 159-177, 2019. [CrossRef] [Google Scholar] [Publisher Link]

[19] Zhang Guojie et al., "Numerical Investigation of Novel Dehumidification Strategies in Nuclear Plant Steam Turbine based on the Modified Nucleation Model," *International Journal of Multiphase Flow*, vol. 120, 2019. [CrossRef] [Google Scholar] [Publisher Link]

[20] Guojie Zhang et al., "Design and Optimization of Novel Dehumidification Strategies Based on Modified Nucleation Model in Three-Dimensional Cascade," *Energy*, vol. 187, 2019. [CrossRef] [Google Scholar] [Publisher Link]

[21] Lihua Cao et al., "Distribution of Condensation Droplets in the Last Stage of Steam Turbine Under Small Flow Rate Condition," *Applied Thermal Engineering*, vol. 181, 2020. [CrossRef] [Google Scholar] [Publisher Link]

[22] Chuang Wen et al., "Numerical Modelling of Wet Steam Flows in Turbine Blades," *Advances in Heat Transfer and Thermal Engineering*, pp. 397-401, 2021. [CrossRef] [Google Scholar] [Publisher Link]

[23] Amir Ebrahimi-Fizik, Esmail Lakzian, and Ali Hashemian, "Entropy Generation Analysis of Wet-Steam Flow with Variation of Expansion Rate using NURBS-based Meshing Technique," *International Journal of Heat and Mass Transfer*, vol. 139, pp. 399-411, 2019. [CrossRef] [Google Scholar] [Publisher Link]

[24] Ali Hashemian, Esmail Lakzian, and Amir Ebrahimi-Fizik, "On the Application of Isogeometric Finite Volume Method in Numerical Analysis of Wet-Steam Flow Through Turbine Cascades," *Computers & Mathematics with Applications*, vol. 79, no. 6, pp. 1687-1705, 2020. [CrossRef] [Google Scholar] [Publisher Link]

[25] "ANSYS Fluent User's Guide," *Fluent*, 2016. [Google Scholar]

[26] "Ansys Fluent 12.0 Theory Guide," *Ansys Inc*, 2009. [Google Scholar] [Publisher Link]

[27] A. Zaleta-Aguilar et al., "Concept on Thermoeconomic Evaluation of Steam Turbines," *Applied Thermal Engineering*, vol. 27, no. 2, pp. 457-466, 2007. [CrossRef] [Google Scholar] [Publisher Link]

[28] C.A. Moses, and G.D. Stein, "On the Growth of Steam Droplets Formed in a Laval Nozzle Using Both Static Pressure and Light Scattering Measurements," *Journal of Fluids Engineering*, vol. 100, no. 3, pp. 311-322, 1978. [CrossRef] [Google Scholar] [Publisher Link]

[29] Sun Lan-xin, Zheng Qun, and Liu Shun-long, "2D-Simulation of Wet Steam Flow in a Steam Turbine with Spontaneous Condensation," *Journal of Marine Science and Application*, vol. 6, pp. 59-63, 2007. [CrossRef] [Google Scholar] [Publisher Link]